nature neuroscience

Lipidomics identifies cardiolipin oxidation as a mitochondrial target for redox therapy of brain injury

Jing Ji[1–4], Anthony E Kline[4–6], Andrew Amoscato[2,3], Alejandro K Samhan-Arias[2,3], Louis J Sparvero[2,3], Vladimir A Tyurin[2,3], Yulia Y Tyurina[2,3], Bruno Fink[7], Mioara D Manole[4,8], Ava M Puccio[9], David O Okonkwo[9], Jeffrey P Cheng[4,5], Henry Alexander[1,4], Robert S B Clark[1,4,8], Patrick M Kochanek[1,4,8], Peter Wipf[10], Valerian E Kagan[2,3] & Hülya Bayır[1–4,8]

The brain contains a highly diversified complement of molecular species of a mitochondria-specific phospholipid, cardiolipin, which, because of its polyunsaturation, can readily undergo oxygenation. Using global lipidomics analysis in experimental traumatic brain injury (TBI), we found that TBI was accompanied by oxidative consumption of polyunsaturated cardiolipin and the accumulation of more than 150 new oxygenated molecular species of cardiolipin. RNAi-based manipulations of cardiolipin synthase and cardiolipin levels conferred resistance to mechanical stretch, an *in vitro* model of traumatic neuronal injury, in primary rat cortical neurons. By applying a brain-permeable mitochondria-targeted electron scavenger, we prevented cardiolipin oxidation in the brain, achieved a substantial reduction in neuronal death both *in vitro* and *in vivo*, and markedly reduced behavioral deficits and cortical lesion volume. We conclude that cardiolipin oxygenation generates neuronal death signals and that prevention of it by mitochondria-targeted small molecule inhibitors represents a new target for neuro-drug discovery.

Every year in the US alone, an estimated 1.7 million people sustain acute brain injury from trauma and, of those, 52,000 die and 85,000 suffer from long-term disabilities[1,2]. This includes injuries from many etiologies, such as road traffic accidents, falls, assaults and sports concussions. In addition, the RAND Corporation estimates that over 400,000 US soldiers have suffered TBI in Operation Iraqi Freedom and Operation Enduring Freedom[3]. A specific therapy for TBI does not yet exist, and standard treatment remains supportive in nature. Like many forms of acute brain injury, TBI involves primary injury, which is felt to be refractory to treatment, and secondary injury, characterized by a cascade of biochemical and cellular events contributing to neuronal damage over time[4]. Secondary injury involves multiple pathways of neuronal death that represent viable therapeutic targets[5,6].

The complexity of brain function requires sophisticated coordination of highly diversified operational signals. Numerous small molecule signals formed from a relatively limited number of metabolic precursors are accountable for the precision and effectiveness of the brain's operational language. Among these are polyunsaturated lipids capable of undergoing enzymatic oxidation and other metabolic conversions yielding oxygenated signaling entities, from eicosanoids, prostanoids and resolvins to cannabinoids and neuroprotectins. There is substantial archaeological evidence that exploitation of abundant food resource enriched in polyunsaturated lipids was essential for sustaining the comparatively large size, apparent unique complexity and high level of interconnectivity in the modern human brain and provided an advantage in multi-generational brain development, thereby making possible the advent of *Homo sapiens*[7]. The demand for diverse polyunsaturated lipid precursors is so large that mitochondria-specific cardiolipin is represented in the brain, but not in other tissues, by hundreds of polyunsaturated individual molecular species[8]. Previously, we found that, in fatally injured cells, oxidation of polyunsaturated cardiolipin species by cytochrome *c* (cyt c) generates death signals that are essential for mitochondrial permeability transition and release of death factors into the cytosol[9].

RESULTS

Cardiolipin oxidation and neuronal death

Although lipid peroxidation has been long associated with acute brain injury, its specific role in mediating damaging pathways and signaling cascades is not well understood[10,11]. We reasoned that aberrant cardiolipin peroxidation may be an important pathogenic pathway in acute brain injury. Using a newly developed two-dimensional liquid chromatography mass spectrometry (2D-LC-MS) protocol, we performed global lipidomics analysis of phospholipids (**Fig. 1a**), which revealed almost 190 individual molecular species of cardiolipin in normal rat brain, of which only ten were oxidized. Notably, experimental TBI, controlled cortical impact (CCI), induced oxidation of the majority of polyunsaturated molecular species of cardiolipin;

[1]Department of Critical Care Medicine, University of Pittsburgh, Pittsburgh, Pennsylvania, USA. [2]Department of Environmental and Occupational Health, University of Pittsburgh, Pittsburgh, Pennsylvania, USA. [3]Center for Free Radical and Antioxidant Health, University of Pittsburgh, Pittsburgh, Pennsylvania, USA. [4]Safar Center for Resuscitation Research, University of Pittsburgh, Pittsburgh, Pennsylvania, USA. [5]Department of Physical Medicine and Rehabilitation, University of Pittsburgh, Pittsburgh, Pennsylvania, USA. [6]Center for Neuroscience, University of Pittsburgh, Pittsburgh, Pennsylvania, USA. [7]Noxygen Science Transfer and Diagnostics GmbH, Elzach, Germany. [8]Children's Hospital of Pittsburgh of University of Pittsburgh Medical Center, Pittsburgh, Pennsylvania, USA. [9]Department of Neurological Surgery, University of Pittsburgh, Pittsburgh, Pennsylvania, USA. [10]Department of Chemistry, University of Pittsburgh, Pittsburgh, Pennsylvania, USA. Correspondence should be addressed to H.B. (bayihx@ccm.upmc.edu).

Received 4 June; accepted 25 July; published online 26 August 2012; corrected online 5 September 2012 (details online); doi:10.1038/nn.3195

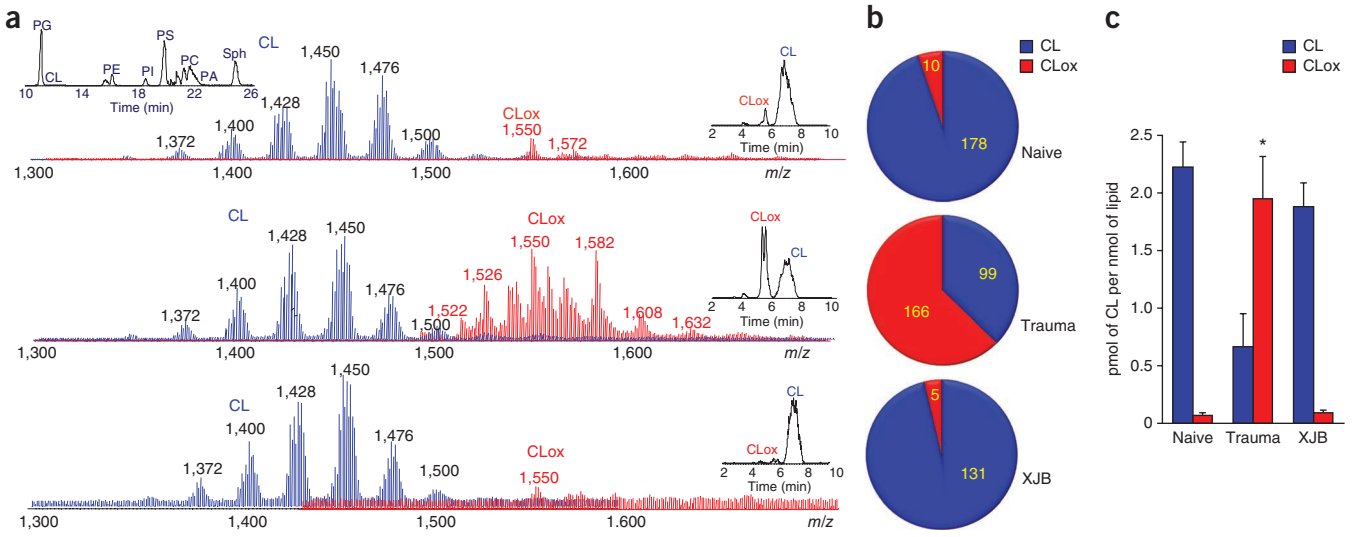

Figure 1 Assessment of molecular species of cardiolipin and its oxidation products by 2D-LC-MS after TBI. (**a**) Typical spectra of cardiolipin (CL) obtained from brain cortex. Top, multiple non-oxidized (8–10 major clusters of mass ions shown in blue) and a few oxidized (shown in red, CLox) clusters of cardiolipin in naive rat. Top left inset, first-dimension chromatographic separation of phospholipids in lipid extracts of the ipsilateral cortex. Cardiolipin eluted during the 10–12-min retention time window. Right insets, second-dimension chromatographic separation of non-oxidized and oxidized cardiolipin. The latter eluted during the 5–6-min retention time window. Middle, non-oxidized (blue) and numerous oxidized (red) cardiolipin species after TBI. Bottom, the effect of XJB-5-131 administration after TBI on the profile of non-oxidized (blue) and oxidized (red) cardiolipin species. PA, phosphatidic acid; PC, phosphatidylcholine; PE, phosphatidylethanolamine; PG, phosphatidylglycerol; PI, phosphatidylinositol; PS, phosphatidylserine; Sph, sphingomyelin. (**b**) Evaluation of the number of non-oxidized and oxidized molecular species of cardiolipin in the brain. (**c**) Quantification of cardiolipin oxidation by 2D-LC-MS. Increased content of CLox at 3 h after CCI and its attenuation by XJB-5-131. $^*P < 0.05$ versus naive and XJB-5-131. Error bars represent s.d. ($n = 4$ rats per group).

the number of non-oxidized cardiolipin species decreased to ~100, whereas that of oxidized species increased to 166 (**Fig. 1b**). Quantitatively, the content of oxidized cardiolipin species increased 20-fold at the expense of decreased amounts of non-oxidized cardiolipin (**Fig. 1c** and **Supplementary Table 1**). This oxidation effect was specific to cardiolipin, as other, more abundant polyunsaturated phospholipids, phosphatidylcholine and phosphatidylethanolamine, remained non-oxidized (**Supplementary Fig. 1**). Clusters of oxidized cardiolipin were also observed in the 2D-LC-MS lipidomics profile in a human brain sample after TBI (**Supplementary Fig. 2**). The scale of CCI-induced oxidative changes in cardiolipin far exceeded the detectable, but much less pronounced, decreases of the levels of glutathione (GSH) and protein sulfhydryls (PSH) in the rat brain (**Supplementary Fig. 3a**,**b**). The decrease in GSH levels after CCI could be associated with responses to accumulation of cardiolipin hydroperoxides by mitochondrial GSH peroxidase IV that are known to catalytically reduce cardiolipin hydroperoxides at the expense of GSH[12,13].

To gain further insight into the role of cardiolipin and its oxidation in CCI induced damage, we used an *in vitro* TBI model of mechanical stretch injury in rat primary cortical neurons. Mechanical stretch triggered robust and selective peroxidation of cardiolipin (**Supplementary Fig. 3c**), but not phosphatidylcholine or phosphatidylethanolamine, which comprise 49% and 30%, respectively, of total phospholipids in primary neurons. Stretch decreased neuronal viability, as assessed by lactate dehydrogenase (LDH), 3-(4,5-dimethylthiazol-2-yl)-2,5-diphenyltetrazolium bromide (MTT) and Trypan blue exclusion assays (**Fig. 2a** and **Supplementary Figs. 4** and **5a**), microtubule-associated protein 2 (MAP-2, neuronal cytoskeleton marker) and cleaved caspase 3 immunostaining (**Supplementary Fig. 5b**,**c**), and measurements of caspase 3/7 activity (**Fig. 2b**), cyt c release (**Fig. 2c**), annexin V and

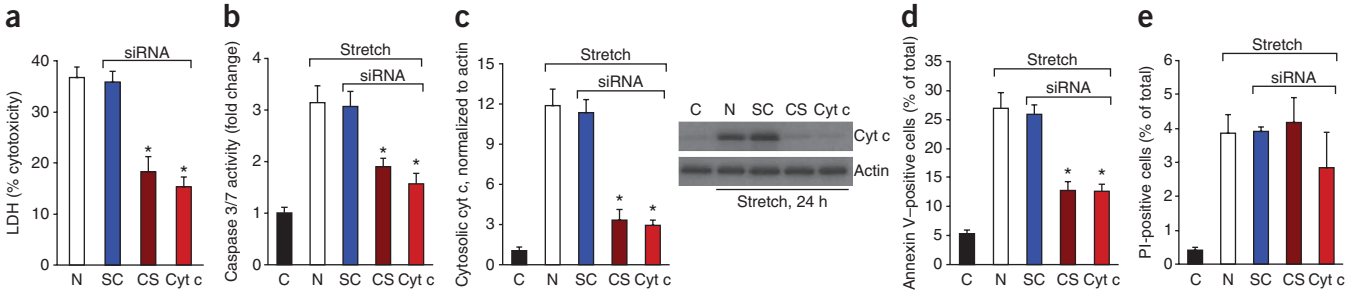

Figure 2 Response of cardiolipin- or cyt c–deficient neurons to *in vitro* TBI. (**a**–**e**) Quantification of cytotoxicity (LDH release) relative to Triton exposure (**a**), caspase 3/7 activity (**b**), cyt c release from mitochondria into cytosol (**c**), annexin V (**d**) and propidium iodide (PI) positivity (**e**) in rat cortical neurons transfected with cardiolipin synthase (CS), cyt c or scrambled control (SC) siRNA after mechanical stretch. Rat cortical neurons were transfected 72 h before mechanical stretch and measurements were obtained at 24 h after stretch injury. C, control normal neurons; N, non-transfected neurons. $^*P < 0.01$ versus non-transfected and scrambled control. Error bars represent s.d. ($n = 4$ experiments). Stretch-induced propidium iodide positivity did not change in cardiolipin- and cyt c–deficient neurons ($P > 0.05$).

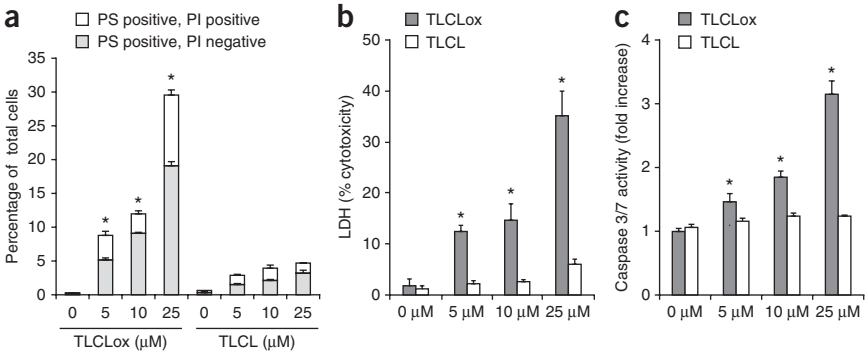

Figure 3 Neuronal cell death in response to non-oxidized and oxidized cardiolipin. (**a**–**c**) Quantification of Annexin V and/or propidium iodide positivity (**a**), cytotoxicity (LDH release) relative to Triton exposure (**b**), and caspase 3/7 activity (**c**) in rat cortical neurons exposed to non-oxidized tetralinoleyl cardiolipin (TLCL) and oxidized TLCL (TLCLox) in the form of liposomes. At three tested concentrations (5, 10 and 25 μM), TLCLox caused dose-dependent cell death in contrast with non-oxidized TLCL. PS, phosphatidylserine. *$P < 0.01$ versus 0 μM and TLCL. Error bars represent s.d. ($n = 3$ experiments).

propidium iodide positivity (**Fig. 2d**,**e**). Notably, exposure of primary neurons to oxidized cardiolipin (but not to non-oxidized cardiolipin) resulted in dose-dependent cell death ($P < 0.01$; **Fig. 3**).

We then used an RNAi approach to manipulate the content of cardiolipin in neurons by knocking down cardiolipin synthase (**Supplementary Fig. 6a**), the key enzyme of *de novo* cardiolipin biosynthesis, and assessed the neurons' responses to stretch. The cardiolipin content decreased to 44% of its level in parental cells (**Supplementary Fig. 6b**), whereas the ATP content did not change (**Supplementary Fig. 6c**). Notably, characteristic markers of stretch-induced cell death, elevated caspase 3/7 activity, release of cyt c from mitochondria into the cytosol, increased annexin V positivity, and release of LDH, were all attenuated and cell survival was increased in cardiolipin-deficient cells (**Fig. 2a–d** and **Supplementary Fig. 5**). Previously, we found that cell death–associated cardiolipin oxidation was catalyzed by peroxidase activity of the cyt c–cardiolipin complex[9]. With this in mind, we generated cyt c–deficient primary neuronal cells (**Supplementary Fig. 6d**) and examined their vulnerability to stretch-induced damage as compared with control cells. Sensitivity of cyt c–deficient neurons to stretch was lower than that of parental cells, as evidenced by caspase 3/7 activity, cyt c release, annexin V positivity and cell viability (**Fig. 2a–d** and **Supplementary Fig. 5**). Taken together, these *in vitro* results are compatible with our hypothesis that cardiolipin oxidation, possibly catalyzed by cyt c, was involved in TBI-induced damage of neurons.

XJB-5-131 targets brain mitochondria

Because mutation or suppression of cardiolipin synthesis and cyt c are therapeutically impractical, we hypothesized that inhibition of cardiolipin peroxidation could attenuate neuronal death and brain injury. This might be achieved by targeting electron scavengers, which will prevent formation of H_2O_2, the fuel for cyt c and cardiolipin peroxidase, in the mitochondria. We designed mitochondria-targeted nitroxide payloads conjugated to selective transporters into mitochondria[14]. We reasoned that these mito-nitroxides could represent effective therapeutic agents for brain injury if they accumulate in mitochondria and prevent oxidative damage, penetrate into the CNS and accumulate in the brain tissue, and display low toxicity and high neuroprotective potential. To this end, we used XJB-5-131 (**Supplementary Fig. 3d**), a conjugate of 4-amino TEMPO and the chemically modified segment of a bacterial membrane targeting antibiotic Gramicidin S, which effectively delivered the nitroxide into mitochondria. The characteristic triplet electron paramagnetic resonance (EPR) signal of Gramicidin S–nitroxide was detected almost

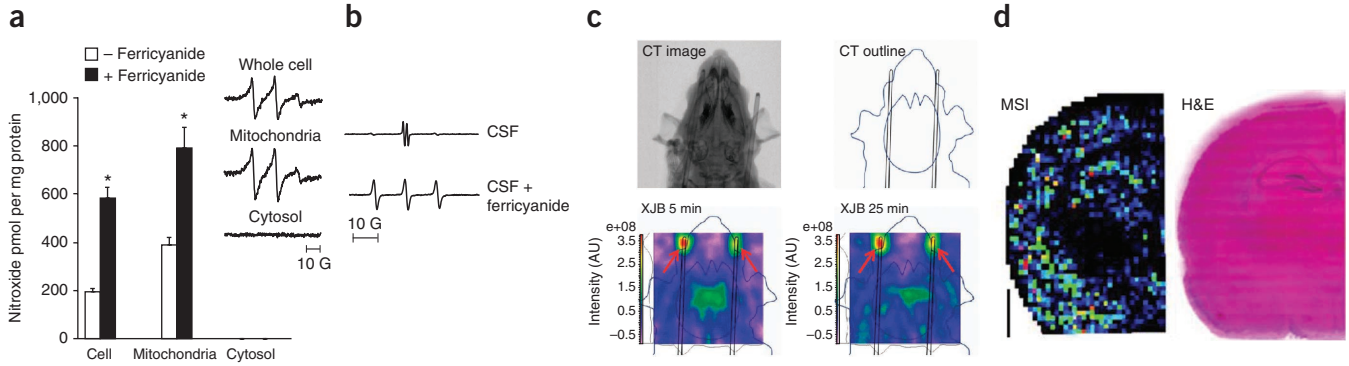

Figure 4 Analysis of XJB-5-131 distribution in neurons and brain. (**a**) XJB-5-131 (10 μM) partitions into mitochondria in primary cortical neurons. Recovered nitroxide radicals in whole cells, mitochondria and cytosol fractions were suspended in phosphate-buffered saline in the presence or absence of 1.5 mM ferricyanide ($K_3Fe(CN)_6$). Inset, representative EPR spectra of XJB-5-131 in different fractions in the presence of ferricyanide. *$P < 0.05$ versus without ferricyanide. Error bars represent s.d. ($n = 4$ experiments). (**b**) EPR-based analysis of XJB-5-131 in CSF in naive rats. A typical ascorbate radical signal (top) was detected by EPR in the absence of ferricyanide. After the addition of ferricyanide, a typical nitroxide signal of XJB-5-131 was detected (bottom). (**c**) Imaging of XJB-5-131 in the brain of naive rats by L-B and EPR spectroscopy. For optimal positioning of the head, micro-computerized tomography (CT) was used (top). Bottom, typical EPR images of XJB-5-131 distribution in the brain obtained at 5 and 25 min after its intravenous injection (50 mg per kg). Arrows indicate two nitroxide radical standards (2.5 and 5 μl of 10 mM 3-carboxy-proxyl solution) placed in proximal portions of capillary tubes. (**d**) Distribution of XJB-5-131 in rat brain assessed by mass spectrometry imaging (MSI) and corresponding hematoxylin and eosin (H&E) staining of the frozen section. XJB-5-131 was detected as the lithium adduct of its hydroxylamine form at *m*/*z* 966 in positive-mode TOF/TOF MSI with 2,5-dihydroxybenzoic acid (DHB) matrix. The black scale bar is 2 mm. The pixels represent a heat map with red being the highest intensity.

exclusively in the mitochondrial fraction of primary cortical neurons treated with XJB-5-131 (**Fig. 4a**), and cell viability was not affected (**Supplementary Fig. 4**).

To evaluate CNS penetration of XJB-5-131, we measured the drug concentration in cerebrospinal fluid (CSF) by EPR spectroscopy. Typical nitroxide signals were detected in CSF when XJB-5-131 (10 mg per kg of body weight) was administered intravenously to naive postnatal day 17 (P17) rats (**Fig. 4b**). At 30 min after injection, the total concentration of nitroxide and its reduced form (revealed in the presence of ferricyanide) in CSF was 1.4 ± 0.1 nM (mean ± s.d.). By employing micro-computerized tomography and L-Band *in vivo* EPR imaging, we documented a time- and dose-dependent distribution of XJB-5-131 in naive P17 rat brains after intravenous injection (**Fig. 4c**). We used mass spectrometric imaging and confirmed the presence of XJB-5-131 in the brain tissue after a single intravenous dose (**Fig. 4d**). Finally, direct quantification of XJB-5-131 in the brain tissue by LC-MS also revealed its accumulation to a level of 16.5 ± 4.3 pmol g^{-1} of tissue (mean ± s.d.) at 3 h after a single 10 mg per kg intravenous injection.

XJB-5-131 protects cardiolipin and improves behavior

We further examined whether XJB-5-131 would inhibit TBI-induced cardiolipin oxidation. We found that cardiolipin oxidation was almost completely blocked by XJB-5-131 administered 10 min after TBI (**Fig. 1**). The number of non-oxygenated and oxygenated species was comparable to those in control brain. Quantitatively, the amounts of non-oxidized and oxidized cardiolipins remained similar to those in the non-traumatized brain (**Fig. 1c**). In addition, XJB-5-131 protected brain thiols, GSH and PSH, oxidized by TBI[15,16] (**Supplementary Fig. 3a**).

Given the ability of XJB-5-131 to protect against cardiolipin oxidation, we evaluated its neuroprotective potential in TBI and performed neurobehavioral testing on P17 rats subjected to CCI injury. We assessed motor function with the well-established beam balance and inclined platform tasks and evaluated cognitive performance using novel object recognition (NOR) and Morris water maze tests, which are sensitive to motor and cognitive function and/or dysfunction after TBI[17–19]. Balancing ability or inclined platform performance did not differ among groups before surgery (**Fig. 5a**,**b**), suggesting that pre-training was consistent among all groups. However, after surgery, a significant improvement in motor performance (with both tasks, $P \leq 0.0001$) was observed on days 3–5 in the sham and CCI + XJB-5-131 groups compared with the CCI + vehicle group (**Fig. 5a**,**b**). Although all groups began at a similar level in the water maze, both the CCI + XJB-5-131 and sham groups performed progressively better than the CCI + vehicle group. This cognitive benefit was observed during both the acute and subchronic phases of training, which correspond to post-injury days 11–15 and 30–34, respectively ($P < 0.001$; **Fig. 5c** and **Supplementary Fig. 7a**). Although the rats treated with XJB-5-131 found the platform significantly faster than vehicle-treated rats ($P < 0.001$, $N = 7$–10 rats per group), the time spent searching in the target quadrant during a single probe trial was not statistically different between the two groups ($P = 0.09$, $N = 7$–10 rats per group). To further assess memory retention, we used the NOR memory test on post-operative day 29. XJB-5-131–treated rats spent significantly more time exploring the novel object than the vehicle-treated rats ($P < 0.01$; **Fig. 5d**). Swim speed did not differ among groups ($P = 0.12$), indicating that water maze or NOR test performance were not influenced by differences in swimming or motor ability or motivational deficits.

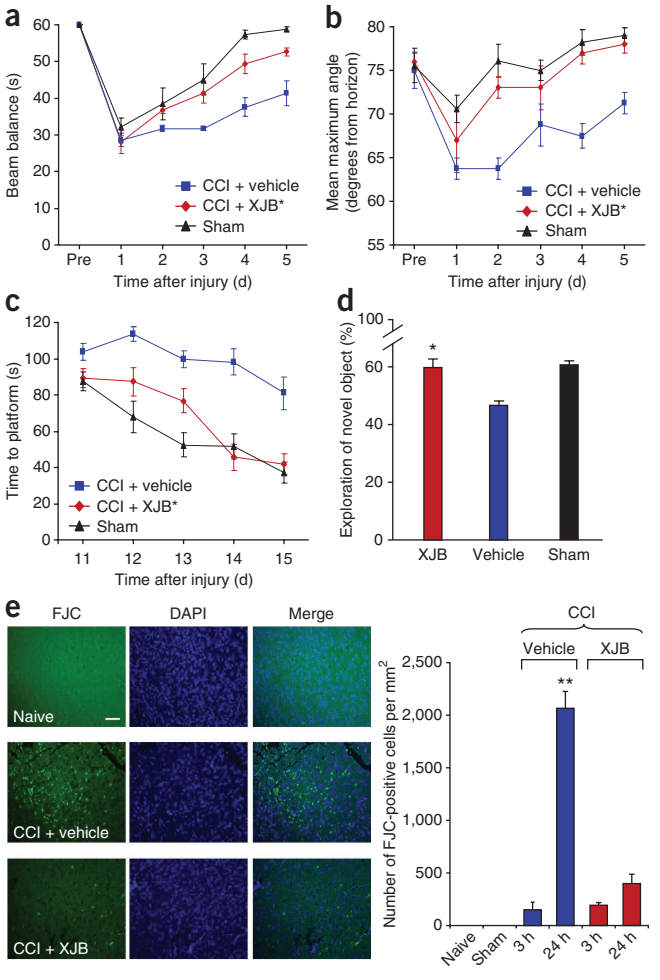

Figure 5 Assessments of neurobehavioral and histological outcome in P17 rats treated with XJB-5-131 after TBI. (**a**) Ability of rats to remain (seconds) on the beam balance apparatus before and after CCI or sham injury. A repeated-measures ANOVA revealed a significant group ($F_{2,15} = 14.452$, $P = 0.0003$), day ($F_{5,75} = 47.631$, $P < 0.0001$) and group by day interaction effect ($F_{10,75} = 2.186$, $P = 0.028$). Bonferroni *post hoc* analyses revealed that the CCI + XJB-5-131 group performed significantly better than the CCI + vehicle group ($P = 0.001$). Error bars represent s.e.m. ($n = 7$–10 rats per group). (**b**) Maximum angle (degrees) for rats to remain on an inclined platform. A repeated-measures ANOVA revealed significant group ($F_{2,15} = 13.164$, $P = 0.0005$), day ($F_{5,75} = 18.085$, $P < 0.0001$) and group by day interaction ($F_{10,75} = 2.902$, $P = 0.004$). Bonferroni *post hoc* analyses revealed that the TBI + XJB-5-131 group performed significantly better than the TBI + vehicle group ($P < 0.001$). Error bars represent s.e.m. ($n = 7$–10 rats per group). (**c**) Latency (s) for rats to locate a hidden (submerged) platform on post-TBI days 11–15. A repeated-measures ANOVA revealed significant group ($F_{2,15} = 19.753$, $P < 0.0001$), day ($F_{4,120} = 22.126$, $P < 0.0001$) and group by day interaction ($F_{8,120} = 2.437$, $P = 0.018$). Bonferroni *post hoc* analyses revealed that the TBI + XJB-5-131 group performed significantly better than the TBI + vehicle group ($P < 0.001$) and did not differ from the sham controls ($P = 0.08$). Error bars represent s.e.m. ($n = 7$–10 rats per group). (**d**) NOR task performance 29 d after sham or CCI injury. TBI + XJB-5-131 rats exhibited a better 24-h delay NOR task performance score than TBI + vehicle rats (*$P < 0.001$, ANOVA, $F_{2,27} = 14.736$). Error bars represent s.e.m. ($n = 9$–10 rats per group). (**e**) Assessment of neurodegeneration by Fluoro-Jade C (FJC) staining. Neurodegeneration observed in the pericontusional area 24 h after CCI was attenuated by XJB-5-131. The white scale bar represents 40 μm. **$P < 0.05$ versus naive and sham controls, CCI 3 h + vehicle and CCI + XJB-5-131. Error bars represent s.d. ($n = 4$ rats per group).

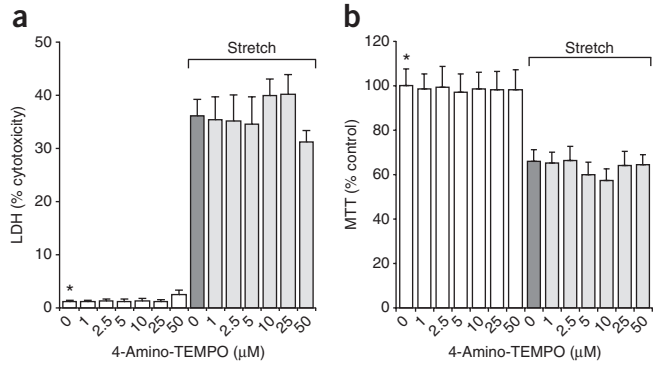

Figure 6 Response of neurons treated with 4-amino-TEMPO to *in vitro* TBI. (**a**) Percentage cytotoxicity (lactate dehydrogenase (LDH) release relative to Triton exposure (corrected for background LDH). (**b**) MTT as a percentage of normal control conditions. Vehicle or 4-amino-TEMPO was added to the medium 10 min before stretch. Mechanical stretch induced approximately 35% neuronal death, as assessed by MTT and LDH at 24 h. $*P < 0.01$ versus stretch neurons. Error bars represent s.d. ($n = 3$ experiments).

XJB-5-131 attenuates apoptotic neuronal death

To evaluate the potency of XJB-5-131 in preventing neuronal death, we employed Fluoro-Jade C staining (**Fig. 5e**), which is commonly used to detect degenerating neurons regardless of the specific cell death pathway[20]. The number of Fluoro-Jade C–positive cells increased at 24 h as compared with 3 h after TBI and naive or sham. Fluoro-Jade C positivity was observed predominantly in the pericontusional area and was significantly attenuated by treatment with XJB-5-131 ($P < 0.05$). Furthermore, cortical lesion volume was significantly decreased at 5 weeks in the TBI group treated with XJB -5-131 as compared with the TBI group that received vehicle ($P < 0.05$; **Supplementary Fig. 7b**).

To better define the possible cell death pathways responsible for neuronal degeneration and the effect of XJB-5-131 *in vivo*, we examined caspase 3/7 activity. Ipsilateral cortical caspase 3/7 activity was increased at 24 h (but not at 3 h) after CCI (**Supplementary Fig. 8**). This effect was attenuated by XJB-5-131, pointing to its anti-apoptotic mechanism of action. Similarly, treatment with XJB-5-131 (5, 10 and 25 μM) attenuated stretch-induced neuronal death (**Supplementary Figs. 4** and **5**) via suppression of mitochondrial superoxide production (**Supplementary Fig. 9a**) and stretch-induced cyt c release into the cytosol (**Supplementary Fig. 9b**). 4-amino-TEMPO, the active nitroxide part of XJB-5-131, but which lacks the mitochondria-targeting hemigramicidin moiety, failed to protect against stretch-induced neuronal death (**Fig. 6**), suggesting that mitochondrial damage was involved in neuronal cell death.

XJB-5-131 acts as an electron scavenger

The two likely mechanisms of XJB-5-131's action in the brain are either as a superoxide dismutase (SOD)-mimetic, catalyzing the dismutation of superoxide radicals into H_2O_2, or as an electron scavenger, preventing one-electron reduction of molecular oxygen to superoxide. In the former case, XJB-5-131 would retain its radical state, whereas in the latter case, XJB-5-131 would be reduced to hydroxylamine. In different redox environments, dynamic interconversions between the nitroxide and hydroxylamine forms occur, resulting in the establishment of an equilibrium between the two. This equilibrium is readily detectable by EPR spectra of the nitroxides (**Fig. 7**). Nitroxide radicals elicit a characteristic EPR signal with hyperfine splitting constants of 16.4 G (a_N). In contrast, hydroxylamines are EPR silent and produce no signals in the spectrum. A characteristic triplet EPR signal (**Fig. 7a**) from nitroxide radicals disappeared and was substituted by a typical doublet signal of ascorbate radicals (with hyperfine splitting constants of 1.84 G) following reduction of nitroxides. This signal of ascorbate radicals disappeared upon addition of ascorbate oxidase. As potent reductants, hydroxylamines are readily oxidized by metalloproteins in their higher valency states (for example, Fe(III)–cyt c) and even more so by their reactive intermediates (for example, oxo-ferryls Fe(IV) = O produced in the presence of H_2O_2). Indeed, addition of oxidized ferri–cytochrome *c* or cyt c/H_2O_2, to hydroxylamine (produced by the ascorbate-driven reduction of the nitroxide with subsequent elimination of excess ascorbate by ascorbate oxidase), resulted in one-electron oxidation of hydroxylamines and re-appearance of the characteristic nitroxide EPR signals.

We also observed these interconversions between hydroxylamines and nitroxides in brain homogenates (**Fig. 7b**). Addition of the nitroxide to brain homogenate produced a typical ascorbate radical signal as a result of the reaction with endogenous ascorbate[16]. After pretreatment of the homogenate with ascorbate oxidase, the addition of the nitroxide immediately yielded the characteristic triplet signal of the nitroxide radical. Notably, triggering NADH-dependent transport of electrons resulted in substantial suppression of the EPR signal of nitroxides as a result of their reduction by electron transport chain. Finally, the redox interconversion between the nitroxide (>N-O*) and hydroxylamine (>N-OH) functionalities is a H^+-dependent process, whereby, in the pH range of 6–7, deprotonation of the hydroxylamine (>N+H-OH) markedly accelerates its auto-oxidation to nitroxide[21,22]. This suggests that, in the basic environment of mitochondria (pH~8.0), targeted XJB-5-131 hydroxylamine will

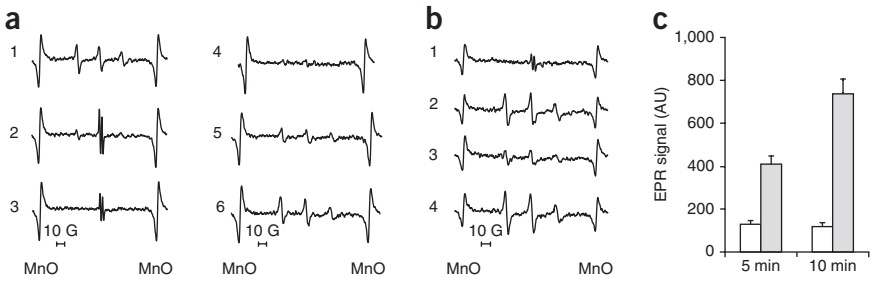

Figure 7 EPR spectroscopy assessment of interconversions of nitroxides and hydroxylamines. (**a**) Effect of ascorbate, ascorbate oxidase and cyt c/H_2O_2 on the EPR signal of XJB-5-131 (1: XJB-5-131 alone in 35 μl of phosphate-buffered saline + 35 μl of DMSO; 2: 1 + 250 μM ascorbate, 1 min; 3: 1 + 250 μM ascorbate, 5 min; 4: 1 + 250 μM ascorbate, 5 min + ascorbate oxidase (1 U, 15 min); 5: 4 + 10 μM cyt c; 6: 4 + 10 μM cyt c/200 μM H_2O_2). (**b**) Effect of ascorbate, ascorbate oxidase and NADH on the EPR signal of XJB-5-131 in brain homogenates (1: 35 μl of brain homogenate (350 μg of protein) in phosphate-buffered saline + 7 μM XJB-5-131 + 35 μl of DMSO; 2: 1 + ascorbate oxidase (2 U), 30 min; 3: 2 + NADH (200 μM), 30 min; 4: 3 + 100 μM $K_3Fe(CN)_6$). (**c**) Effect of pH on the EPR signal of XJB-5-131-OH. We mixed 50 μl of 7 μM XJB-5-131-OH in DMSO with either 50 μl of 50 μM HEPES (pH 7.45, open bars) or 50 μl of 50 μM HEPES (pH 8.25, filled bars). Error bars represent s.d.

spontaneously undergo auto-oxidation to the respective nitroxide (**Fig. 7c**). Furthermore, using LC-MS–based quantification, we found that nearly all XJB-5-131 (91.7 ± 14.5%) was present in the hydroxylamine form and the nitroxide represented only a small fraction of total XJB-5-131. Given that the hemigramicidin S–derived alkene peptide isostere sequence in XJB-5-131 is responsible for its predominant localization in mitochondria, its action likely occurs through the scavenging of electrons leaking from discoordinated electron carriers, rather than through involvement of SOD-like activity.

DISCUSSION

For decades, oxidative stress has been implicated in acute brain injury[10,23,24], which has prompted some of the earliest randomized controlled trials in the field of TBI[25]. However, limitations with specificity, potency, blood-brain barrier and/or cell penetration with conventional antioxidant approaches may have contributed to these past treatment failures[26]. Our results identify selective peroxidation of cardiolipin as an important pathogenic mechanism for TBI. The peroxidation process yields a high diversity of oxidized cardiolipin products that may be required to activate the neuronal death program.

Redistribution of cardiolipin from the inner mitochondrial membrane to the outer mitochondrial membrane and subsequent accumulation of cardiolipin oxidation products, catalyzed by cyt c, are required stages in the execution of the intrinsic apoptotic program[9,27–31]. Oxidized cardiolipin (but not non-oxidized cardiolipin) causes the release of pro-apoptotic factors, including cyt c, from mitochondria into the cytosol and caspase activation[32]. The mechanisms of mitochondrial membrane permeabilization triggered by oxidized cardiolipin may involve interactions with several outer membrane proteins (for example, Bax, Bak and VDAC)[33–35]. It is likely that cardiolipin peroxidation is not a result of the aftermath of cell death, but is instead causative to it, thus offering an opportunity for a targeted therapy. Indeed, we found that mitochondrial delivery of small molecule inhibitors, electron scavengers, led to the prevention of both accumulation of a large number of cardiolipin oxidation products, as well as brain damage. The use of the mitochondria-targeted nitroxides offers considerable therapeutic advantages compared with previously used strategies, in terms of getting to the source of oxidative stress at an early point with the highest specificity and the least toxicity and possibly limiting deleterious effects on oxidative signaling in other brain lipids.

Stable nitroxide radicals combine electron and free radical scavenging actions with SOD-mimicking and recycling capacities. One of these nitroxides, Tempol, has been shown to improve motor function after experimental TBI[36]; however, high millimolar concentrations were required to attain this improvement. Depending on the redox environment, nitroxides may be present in three major forms: oxidized (oxoammonium cation, $RN^+ = O$), semi-reduced (the nitroxide radical, RN-O•) and reduced (the hydroxylamine, RN-OH)[37]. Accordingly, there are three major biochemical mechanisms of action for nitroxides. First, superoxide anion-radical–driven interconversions between 1↔2 underlie the SOD-mimicking activity of nitroxides[38]. This catalytic activity regenerates the nitroxide form of the compound; no reduced form, hydroxylamine, is produced in this reaction. Second, electron scavenging occurs from other reductants, particularly reduced respiratory complexes of mitochondria. This mechanism prevents leakage of electrons from electron transport chains to molecular oxygen (thus, the formation of superoxide radicals) and yields hydroxylamines via a one-electron reduction process. In extra-mitochondrial compartments, ascorbate is the most abundant low molecular weight reductant of nitroxides, whereas the reactivity of GSH and other thiols is much lower[39]. Third, interactions of hydroxylamines with oxidizing radicals, oxidized intermediates of peroxidases, or oxidized forms of transition metals or metalloproteins yield the nitroxide. For example, reduction of hydroxylamines by oxidizing radicals, such as peroxyl, alkoxyl or ferri–cytochrome *c*, converts hydroxylamines back to their nitroxide forms[22,40,41]. We performed EPR spectroscopy to more clearly illustrate these interconversions of nitroxides and hydroxylamines. Notably, these interconversions between hydroxylamines and nitroxides can be observed in brain homogenates.

It is known that the immature brain has compromised antioxidant defenses compared with adults[42], implying that the beneficial effects of XJB-5-131 could potentially be magnified in the developing brain. Given the enormous burden of TBI in pediatrics, our use of a developmental TBI model may be of additional clinical relevance. Germane to our findings, considerable mitochondrial dysfunction with altered bioenergetics[43], increased oxidative stress markers[44], membrane permeabilization[45] and release of proapoptotic factors[46] have been observed in both experimental models and humans after severe TBI. There is accumulating evidence supporting a role of TBI as a trigger for a number of neurodegenerative diseases, such as dementia[47], amyotrophic lateral sclerosis and Parkinson's disease[48]. Given the role of oxidative stress across the field of brain injury, our results suggest that cardiolipin peroxidation may be characteristic of other types of acute brain injury, such as that seen in stroke and cardiac arrest. Thus, this mechanism and the linked new therapeutic approach are relevant to other forms of CNS injury.

METHODS

Methods and any associated references are available in the online version of the paper.

Note: Supplementary information is available in the online version of the paper.

ACKNOWLEDGMENTS

The authors would like to thank J. Lewis for the technical assistance of unbiased stereology for cortical lesion volume, J. Davoren for the preparation of XJB-5-131 and Y.M. Frapart (Laboratoire de Chimie Biochimie Pharmacologique et Toxicologique, Université Paris Descartes) for providing an L-band EPR spectrometer for *in vivo* imaging. This study was supported in part by grants from the US National Institutes of Health (NS061817 (H.B.), NS060005 (A.E.K.), HL070755 (V.E.K.), ES020693 (Y.Y.T. and V.E.K.), NS076511 and U19AI068021 (H.B. and V.E.K.)), the US National Institute for Occupational Safety and Health (OH008282 to V.E.K.) and the US Army (W81XWH-09-0187 to P.M.K.). A.K.S.-A. is a recipient of a research fellowship from La Junta de Extremadura y el Fondo Social Europeo (2010063090).

AUTHOR CONTRIBUTIONS

J.J. designed and performed experiments, analyzed data and wrote the manuscript. A.E.K. and J.P.C. contributed to the neurocognitive outcome assessment and writing of the manuscript. A.A., Y.Y.T. and A.K.S.-A. contributed to the assessment of cardiolipin oxidation by 2D-LC-MS. L.J.S. contributed to the mass spectrometry imaging. V.A.T. contributed to the EPR measurements. B.F. contributed to the *in vivo* EPR imaging. M.D.M. contributed to the unbiased stereology for cortical lesion volume. A.M.P. and D.O.O. contributed to evaluation of human TBI tissue and writing of the manuscript. H.A. performed *in vivo* TBI experiments. R.S.B.C. and P.M.K. contributed to data analysis and manuscript writing. P.W. contributed to the preparation of XJB-5-131 and manuscript writing. V.E.K. and H.B. initiated and directed the entire study, designed experiments and wrote the manuscript.

COMPETING FINANCIAL INTERESTS

The authors declare no competing financial interests.

Published online at http://www.nature.com/doifinder/10.1038/nn.3195.
Reprints and permissions information is available online at http://www.nature.com/reprints/index.html.

1. Faul, M., Xu, L., Wald, M.M. & Coronado, V.G. *Traumatic Brain Injury in the United States: Emergency Department Visits, Hospitalizations and Deaths 2002–2006* (Centers for Disease Control and Prevention, National Center for Injury Prevention and Control, Atlanta, Georgia, 2010).

2. Thurman, D.J., Alverson, C., Dunn, K.A., Guerrero, J. & Sniezek, J.E. Traumatic brain injury in the United States: a public health perspective. *J. Head Trauma Rehabil.* **14**, 602–615 (1999).
3. RAND. Invisible Wounds of War Study. <http://www.rand.org/multi/military/veterans.html> (26 June 2011).
4. Ghajar, J. Traumatic brain injury. *Lancet* **356**, 923–929 (2000).
5. Maas, A.I., Roozenbeek, B. & Manley, G.T. Clinical trials in traumatic brain injury: past experience and current developments. *Neurotherapeutics* **7**, 115–126 (2010).
6. Stoica, B.A. & Faden, A.I. Cell death mechanisms and modulation in traumatic brain injury. *Neurotherapeutics* **7**, 3–12 (2010).
7. Broadhurst, C.L. *et al.* Brain-specific lipids from marine, lacustrine, or terrestrial food resources: potential impact on early African *Homo sapiens*. *Comp. Biochem. Physiol. B Biochem. Mol. Biol.* **131**, 653–673 (2002).
8. Kiebish, M.A. *et al.* Lipidomic analysis and electron transport chain activities in C57BL/6J mouse brain mitochondria. *J. Neurochem.* **106**, 299–312 (2008).
9. Kagan, V.E. *et al.* Cytochrome c acts as a cardiolipin oxygenase required for release of proapoptotic factors. *Nat. Chem. Biol.* **1**, 223–232 (2005).
10. Chan, P.H. & Fishman, R.A. Transient formation of superoxide radicals in polyunsaturated fatty acid–induced brain swelling. *J. Neurochem.* **35**, 1004–1007 (1980).
11. Verweij, B.H. *et al.* Impaired cerebral mitochondrial function after traumatic brain injury in humans. *J. Neurosurg.* **93**, 815–820 (2000).
12. Nomura, K., Imai, H., Koumura, T., Kobayashi, T. & Nakagawa, Y. Mitochondrial phospholipid hydroperoxide glutathione peroxidase inhibits the release of cytochrome c from mitochondria by suppressing the peroxidation of cardiolipin in hypoglycaemia-induced apoptosis. *Biochem. J.* **351**, 183–193 (2000).
13. Ran, Q. *et al.* Transgenic mice overexpressing glutathione peroxidase 4 are protected against oxidative stress–induced apoptosis. *J. Biol. Chem.* **279**, 55137–55146 (2004).
14. Wipf, P. *et al.* Mitochondrial targeting of selective electron scavengers: synthesis and biological analysis of hemigramicidin-TEMPO conjugates. *J. Am. Chem. Soc.* **127**, 12460–12461 (2005).
15. Bayir, H. *et al.* Selective early cardiolipin peroxidation after traumatic brain injury: an oxidative lipidomics analysis. *Ann. Neurol.* **62**, 154–169 (2007).
16. Bayir, H. *et al.* Assessment of antioxidant reserves and oxidative stress in cerebrospinal fluid after severe traumatic brain injury in infants and children. *Pediatr. Res.* **51**, 571–578 (2002).
17. Hamm, R.J. *et al.* Cognitive deficits following traumatic brain injury produced by controlled cortical impact. *J. Neurotrauma* **9**, 11–20 (1992).
18. Kline, A.E., Massucci, J.L., Ma, X., Zafonte, R.D. & Dixon, C.E. Bromocriptine reduces lipid peroxidation and enhances spatial learning and hippocampal neuron survival in a rodent model of focal brain trauma. *J. Neurotrauma* **21**, 1712–1722 (2004).
19. Scafidi, S., Racz, J., Hazelton, J., McKenna, M.C. & Fiskum, G. Neuroprotection by acetyl-L-carnitine after traumatic injury to the immature rat brain. *Dev. Neurosci.* **32**, 480–487 (2010).
20. Schmued, L.C., Stowers, C.C., Scallet, A.C. & Xu, L. Fluoro-Jade C results in ultra high resolution and contrast labeling of degenerating neurons. *Brain Res.* **1035**, 24–31 (2005).
21. Stoyanovsky, D.A. & Cederbaum, A.I. ESR and HPLC-EC analysis of ethanol oxidation to 1-hydroxyethyl radical: rapid reduction and quantification of POBN and PBN nitroxides. *Free Radic. Biol. Med.* **25**, 536–545 (1998).
22. Zhang, R., Goldstein, S. & Samuni, A. Kinetics of superoxide-induced exchange among nitroxide antioxidants and their oxidized and reduced forms. *Free Radic. Biol. Med.* **26**, 1245–1252 (1999).
23. Siesjö, B.K. Cell damage in the brain: a speculative synthesis. *J. Cereb. Blood Flow Metab.* **1**, 155–185 (1981).
24. Wei, E.P., Kontos, H.A., Dietrich, W.D., Povlishock, J.T. & Ellis, E.F. Inhibition by free radical scavengers and by cyclooxygenase inhibitors of pial arteriolar abnormalities from concussive brain injury in cats. *Circ. Res.* **48**, 95–103 (1981).
25. Muizelaar, J.P. *et al.* Improving the outcome of severe head injury with the oxygen radical scavenger polyethylene glycol–conjugated superoxide dismutase: a phase II trial. *J. Neurosurg.* **78**, 375–382 (1993).
26. Lo, E.H., Singhal, A.B., Torchilin, V.P. & Abbott, N.J. Drug delivery to damaged brain. *Brain Res. Brain Res. Rev.* **38**, 140–148 (2001).
27. Sorice, M. *et al.* Cardiolipin and its metabolites move from mitochondria to other cellular membranes during death receptor–mediated apoptosis. *Cell Death Differ.* **11**, 1133–1145 (2004).
28. Nakagawa, Y. Initiation of apoptotic signal by the peroxidation of cardiolipin of mitochondria. *Ann. NY Acad. Sci.* **1011**, 177–184 (2004).
29. Ott, M., Robertson, J.D., Gogvadze, V., Zhivotovsky, B. & Orrenius, S. Cytochrome c release from mitochondria proceeds by a two-step process. *Proc. Natl. Acad. Sci. USA* **99**, 1259–1263 (2002).
30. Zhao, Z. *et al.* Protection of pancreatic beta-cells by group VIA phospholipase A(2)–mediated repair of mitochondrial membrane peroxidation. *Endocrinology* **151**, 3038–3048 (2010).
31. Petrosillo, G., Moro, N., Paradies, V., Ruggiero, F.M. & Paradies, G. Increased susceptibility to Ca^{2+}-induced permeability transition and to cytochrome c release in rat heart mitochondria with aging: effect of melatonin. *J. Pineal Res.* **48**, 340–346 (2010).
32. Petrosillo, G., Casanova, G., Matera, M., Ruggiero, F.M. & Paradies, G. Interaction of peroxidized cardiolipin with rat-heart mitochondrial membranes: induction of permeability transition and cytochrome c release. *FEBS Lett.* **580**, 6311–6316 (2006).
33. Korytowski, W., Basova, L.V., Pilat, A., Kernstock, R.M. & Girotti, A.W. Permeabilization of the mitochondrial outer membrane by Bax/truncated Bid (tBid) proteins as sensitized by cardiolipin hydroperoxide translocation: mechanistic implications for the intrinsic pathway of oxidative apoptosis. *J. Biol. Chem.* **286**, 26334–26343 (2011).
34. Betaneli, V., Petrov, E.P. & Schwille, P. The role of lipids in VDAC oligomerization. *Biophys. J.* **102**, 523–531 (2012).
35. Rostovtseva, T.K., Kazemi, N., Weinrich, M. & Bezrukov, S.M. Voltage gating of VDAC is regulated by nonlamellar lipids of mitochondrial membranes. *J. Biol. Chem.* **281**, 37496–37506 (2006).
36. Deng-Bryant, Y., Singh, I.N., Carrico, K.M. & Hall, E.D. Neuroprotective effects of tempol, a catalytic scavenger of peroxynitrite-derived free radicals, in a mouse traumatic brain injury model. *J. Cereb. Blood Flow Metab.* **28**, 1114–1126 (2008).
37. Wilcox, C.S. & Pearlman, A. Chemistry and antihypertensive effects of tempol and other nitroxides. *Pharmacol. Rev.* **60**, 418–469 (2008).
38. Mitchell, J.B. *et al.* Biologically active metal-independent superoxide dismutase mimics. *Biochemistry* **29**, 2802–2807 (1990).
39. Bobko, A.A., Kirilyuk, I.A., Grigor'ev, I.A., Zweier, J.L. & Khramtsov, V.V. Reversible reduction of nitroxides to hydroxylamines: roles for ascorbate and glutathione. *Free Radic. Biol. Med.* **42**, 404–412 (2007).
40. Soule, B.P. *et al.* The chemistry and biology of nitroxide compounds. *Free Radic. Biol. Med.* **42**, 1632–1650 (2007).
41. Trnka, J., Blaikie, F.H., Smith, R.A. & Murphy, M.P. A mitochondria-targeted nitroxide is reduced to its hydroxylamine by ubiquinol in mitochondria. *Free Radic. Biol. Med.* **44**, 1406–1419 (2008).
42. Fan, P., Yamauchi, T., Noble, L.J. & Ferriero, D.M. Age-dependent differences in glutathione peroxidase activity after traumatic brain injury. *J. Neurotrauma* **20**, 437–445 (2003).
43. Scheff, S.W. & Sullivan, P.G. Cyclosporin A significantly ameliorates cortical damage following experimental traumatic brain injury in rodents. *J. Neurotrauma* **16**, 783–792 (1999).
44. Singh, I.N., Sullivan, P.G. & Hall, E.D. Peroxynitrite-mediated oxidative damage to brain mitochondria: protective effects of peroxynitrite scavengers. *J. Neurosci. Res.* **85**, 2216–2223 (2007).
45. Alessandri, B. *et al.* Cyclosporin A improves brain tissue oxygen consumption and learning/memory performance after lateral fluid percussion injury in rats. *J. Neurotrauma* **19**, 829–841 (2002).
46. Lewén, A. *et al.* Oxidative stress-dependent release of mitochondrial cytochrome c after traumatic brain injury. *J. Cereb. Blood Flow Metab.* **21**, 914–920 (2001).
47. DeKosky, S.T., Ikonomovic, M.D. & Gandy, S. Traumatic brain injury—football, warfare and long-term effects. *N. Engl. J. Med.* **363**, 1293–1296 (2010).
48. McKee, A.C. *et al.* TDP-43 proteinopathy and motor neuron disease in chronic traumatic encephalopathy. *J. Neuropathol. Exp. Neurol.* **69**, 918–929 (2010).

ONLINE METHODS

XJB-5-131 preparation and assessment of XJB-5-131 by EPR spectroscopy were performed as previously described[14]. All surgical, injury and animal care procedures were approved by the University of Pittsburgh Institutional Animal Care and Use Committee.

CCI model. We induced *in vivo* TBI by CCI to the left parietal cortex in P17 rats as described previously[15]. For all studies, a 6-mm metal pneumatically driven impactor tip was used. The velocity of the impact was 4.0 ± 0.2 m s^{-1}, with a penetration depth of 2.5 mm.

XJB-5-131 treatment in P17 rats and assessment of biochemical markers. Rats were randomized into one of the following groups: naive, sham plus vehicle, sham plus XJB-5-131, CCI plus vehicle and CCI plus XJB-5-131. For the XJB-5-131 treatment group, rats were treated with XJB-5-131 (10 mg per kg per dose) administered intravenously at 5 min and intraperitoneally at 24 h after CCI. Rats in the CCI plus vehicle and sham plus vehicle groups received similar treatment, except that XJB-5-131 was replaced with an equal volume of vehicle (50:50, vol/vol, cremophorel:ethanol dissolved in saline (1:3)). Caspase 3/7 activity and GSH and PSH measurements were performed as described[15].

Primary cortical neuronal culture, *in vitro* TBI model and XJB-5-131 treatment. Primary cortical neuronal culture, cell viability assays, assessment of mitochondrial superoxide production with MitoSOX, phosphatidylserine externalization, cytochrome *c* release assay, immunocytochemical staining and *in vitro* TBI model were performed as previously described[49]. Preparation of tetra-linoleoyl-cardiolipin and oxidized tetra-linoleoyl-cardiolipin liposomes was performed as described[9]. Neurons were incubated with XJB-5-131 (concentrations ranging from 1–25 μM) or vehicle 10 min before mechanical stretch.

Cardiolipin synthase and cyt c RNA interference. Small interfering RNA (siRNA) targeting rat cardiolipin synthase, cyt c and pooled scrambled control siRNA were purchased commercially (Life Technologies). Primary neurons were transfected on day 4 with 45 nmol of cardiolipin synthase or cyt c or control siRNA using Lipofectamine 2000 (Invitrogen). The efficacy of cardiolipin synthase and cyt c knockdown was assessed by western blot using antibody to cardiolipin synthase (customized antibody made by Invitrogen, 1:200, clone 8710) and cyt c (BD Pharmingen, 1:1,000, clone 7H8.2C12). Experiments were performed 72 h after transfection.

EPR-based analysis of partitioning and distribution of nitroxides in cultured neurons and in CSF. Primary cortical neurons (7 d *in vitro*, 5×10^6 cells per well) were incubated with 10 μM XJB-5-131 for 15 min at 37 °C. At the end of incubation, cells were washed twice with serum-free medium. Mitochondria-enriched fractions were obtained using a mitochondria isolation kit (Pierce). CSF was collected from the cisterna magna of naive P17 rats 30 min after intravenous injection of XJB-5-131 (10 mg per kg). Each cellular fraction (whole cell pellet, mitochondria and cytoplasm) or CSF was mixed with DMSO (1:1, vol/vol) or 1.5 mM potassium ferricyanide to convert nitroxides to EPR-detectable radical forms. An aliquot of 70 μl of the cellular fraction or CSF was loaded into Teflon tubing (0.8-mm internal diameter, Alpha Wire), which was folded in half and placed into an open ESR quartz tube (inner diameter of 3.0 mm). EPR measurements were made in triplicate using a JEOL-RE1X EPR spectrometer (Jeol) with the following conditions: 334.7-mT center field, 5-mT sweep width, 0.079-mT field modulation, 20-mW microwave power, 0.1-s time constant and 2-min scan time at 22.5 °C. Using signal magnitude and isolated volumes, the amount and concentration of XJB-5-131 were calculated for each sample.

***In vivo* EPR imaging of distribution of nitroxides in the rat brain.** L-Band EPR spectroscopy and micro-computerized tomography were applied for the co-imaging of XJB-5-131 spin label in the brains of naive P17 rats. After intravenous injection of XJB-5-131 (50 mg per kg) or vehicle into P17 rats, the heads of the rats were imaged every 15 min using ELEXSYS E540 L-Band spectrometer and 23-mm resonator (Bruker Biospin GmbH), assuring a high filling factor (sensitivity) for small animals. For observation of spin label spatial distribution in brain tissue, the images were obtained in the presence of two capillaries filled with 2.5 and 5 μl of 10 mM 3-carboxy-proxyl solution. Acquisition of EPR data were accomplished using following settings: modulation amplitude = 2 G, modulation frequency = 100 kHz, microwave power = 40 mW, conversion time = 30 ms, image field of view = 25 mm, acquired angles = 31 and gradient = 24 G cm^{-1}. Finally, we proceeded with the creation of two-dimensional EPR by employing the following strategies: zero order baseline correction, Fourier transform deconvolution using a gaussian window with a width of 0.15 mm and filtered back projection.

Imaging of nitroxides in rat brain by matrix-assisted laser desorption ionization (MALDI) mass spectrometry. Tissue samples were prepared as described previously[50]. Briefly, rats were killed 30 min after a single intravenous injection of XJB-5-131 (10 mg per kg). The brains were dissected and immediately flash frozen in liquid nitrogen. Subsequently, tissues were cut without fixation or embedding. Minimal OCT (Sakura FineTek) was used only to attach the tissue to the cryostat block, and at no time did the blade touch the OCT. Coronal sections (10 μm thick) were cut at −19 °C at and placed onto indium-tin oxide–coated MALDI slides (Delta Technologies). Prepared slides were immediately vacuum-dried for at least 1 h, and stored at −20 °C until matrix application and subsequent mass spectrometry imaging analysis. The adjacent 10-μm-thick brain section was counter-stained with hematoxylin and eosin. Tissue slices were incubated with phospholipase C (PLC) at 3.3 mU μl^{-1} for 20 min at 20–24 °C to remove interference from cationic phospholipid signals. The PLC solution was then carefully pipetted off, followed by two washes with 0.5 M lithium acetate and overnight vacuum drying. As such, XJB-5-131 was subsequently detected as its lithium adduct at *m/z* 966. The MALDI matrix DHB (98%+ grade, Sigma-Aldrich) was freshly dissolved (55 mg ml^{-1} in 70% methanol/0.02% trifluoroacetic acid, vol/vol) before use and was applied with a commercial airbrush (1-s burst every 30 s, with 15 min of spraying followed by 15 min of vacuum drying, total of 90 bursts per slide). Mass spectrometry imaging was carried out in reflector-positive mode using an Autoflex MALDI TOF/TOF (Bruker Daltonics) with a Smartbeam laser focused to approximately 50 μm. The raster scan was performed automatically at a data point interval of 200 μm with a random walk in each area to gain the most signal possible. This yielded approximately 1,750 data points for analysis by FlexImaging 3.0 software (Bruker Daltonics).

Assessment of cardiolipin oxidation by 2D-LC-MS. Total lipids were extracted using the Folch procedure[51] from crude brain mitochondrial fraction. Lipids were analyzed in the first dimension by normal phase chromatography on a Luna silica column (2.0 mm (inner diameter) × 15 cm, Phenomenex). Solvent A consisted of chloroform, methanol and 30% ammonium hydroxide (80:19.5:0.5, vol/vol/vol) and solvent B consisted of chloroform, methanol, water and 30% ammonium hydroxide (60:34:5.5:0.5, vol/vol/vol/vol). Flow was maintained at 0.2 ml min^{-1} and a linear gradient of 0–100% solvent B was run in 30 min. Eighty percent of the flow was diverted to a fraction collector while the remainder was used for mass spectrometry analysis. Individual phospholipid classes from the first dimension chromatography were subsequently analyzed in a second dimension system. For cardiolipin, a C8 column was used (5 μm, 4.6 mm × 15 cm, Phenomenex) with an isocratic solvent system consisting of 2-propanol: water: triethylamine: acetic acid (45:5:0.25:0.25). Flow was maintained at 0.4 ml min^{-1} and analysis was performed on a Waters Premier Q-TOF mass spectrometer. For the remaining phospholipids and for quantitative purposes for cardiolipin, lipids were analyzed on an ion trap instrument (LCQ-Duo, Thermo-Finnigan) using a C18 column (4.6 mm × 15 cm, Phenomenex) with a solvent system consisting of solvent C (acetonitrile, water, triethylamine and acetic acid, 45:5:0.25:0.25) and solvent D (2-propanol, water, triethylamine and acetic acid, 45:5:0.25:0.25) using a linear gradient from 50–80% solvent D in 15 min and ramping to 100% solvent D by 30 min, modified from a previously described system[52,53]. Flow was maintained at 0.4 ml min^{-1}. Instrument conditions for the Waters Premier Q-TOF mass spectrometer were as follows: capillary voltage = 2.85 kV (negative mode), source temperature = 100 °C, desolvation gas = 400 l h^{-1}, sampling cone = 60 V, extraction cone = 4.5 V and ion guide = 3.0 V. Tuning was optimized for all lipids across the scan range. Instrument conditions for the ion trap analysis were as follows: capillary temperature = 250 °C, spray voltage = 4.5 kV and sheath gas = 30. All other tuning parameters were optimized for each individual lipid class.

Neurocognitive outcome assessment. Neurocognitive outcome was assessed by an observer blinded to experimental groups. Motor function was evaluated using the beam balance and inclined plane tests on days 1–5 after CCI or sham injury,

doi:10.1038/nn.3195

as described previously[54]. A water maze task was used to assess spatial learning. Briefly, the maze consisted of a plastic pool (180 cm in diameter, 60 cm high) filled with water (26 ± 1 °C) to a depth of 28 cm and situated in a room with salient visual cues that remained constant throughout the experiment. The platform was a clear Plexiglas stand (10 cm in diameter, 26 cm high) that was positioned 26 cm from the maze wall in the southwest quadrant and held constant throughout the experiment for each animal. Acquisition of spatial learning began on post-operative day 11 and consisted of providing a block of four daily trials for five consecutive days (days 11–15) to locate the platform when it was submerged 2 cm below the water surface. Each trial lasted until either the rat climbed onto the platform or 120 s had elapsed, whichever occurred first. Rats that failed to locate the goal in the designated time were manually guided to it. All animals remained on the platform for 30 s before being placed in a heated incubator between trials (4-min intertrial interval).

In a separate group of rats, assessments of neurocognitive function was performed using a NOR test on days 28–29 and the Morris water maze test on days 30–34 after sham or CCI injury. The NOR test was performed as described previously[19]. Briefly, for the habituation phase, which was conducted 28 d after CCI injury, two similar objects were placed into the inner arena across from where the rat was placed. The rats were allowed to investigate for 35 min to become familiar with the objects. Exploration was defined as sniffing and/or touching the objects. The rats were returned to their home cages at the end of the habituation period, and 24 h later (that is, post-injury day 29) were again placed in the arena with the objects for 1 min before being returned briefly to their home cages. The recognition test was conducted 1 h later and consisted of one of the familiar objects being replaced with a novel object, followed by recording the time spent exploring the original versus novel object. The data were obtained using a spontaneous motor activity recording and tracking system (San Diego Instruments).

Histological assessment. Fluoro-Jade C staining was performed as described[55]. Cortical lesion volume was evaluated by unbiased stereology using a computerized stereology system (Stereologer, Stereology Resource Center) as described[19,56].

Statistical analysis. Statistical analyses of functional outcome were performed using Statview 5.0.1 software (Abacus Concepts). The motor and cognitive data were analyzed by repeated-measures analysis of variance. When the overall ANOVA revealed a significant effect, the data were further analyzed with the Bonferroni/Dunn *post hoc* test to determine specific group differences. The behavioral data and cortical lesion volume are presented as the mean ± s.e.m. and are considered significant when corresponding P values are < 0.05 or as determined by the Bonferroni/Dunn statistic after adjusting for multiple comparisons. All other data were expressed as mean ± s.d. Data involving primary cortical neurons were obtained from at least three independent experiments. Statistical comparisons between groups were performed by Student's t test. Differences were considered statistically significant when P value was < 0.05 and are indicated in figure legends.

49. Ji, J. *et al.* Mitochondrial injury after mechanical stretch of cortical neurons *in vitro*: biomarkers of apoptosis and selective peroxidation of anionic phospholipids. *J. Neurotrauma* **29**, 776–788 (2012).
50. Koizumi, S. *et al.* Imaging mass spectrometry revealed the production of lysophosphatidylcholine in the injured ischemic rat brain. *Neuroscience* **168**, 219–225 (2010).
51. Folch, J., Lees, M. & Sloane Stanley, G.H. A simple method for the isolation and purification of total lipides from animal tissues. *J. Biol. Chem.* **226**, 497–509 (1957).
52. Minkler, P.E. & Hoppel, C.L. Separation and characterization of cardiolipin molecular species by reverse-phase ion pair high-performance liquid chromatography-mass spectrometry. *J. Lipid Res.* **51**, 856–865 (2010).
53. Kim, J., Minkler, P.E., Salomon, R.G., Anderson, V.E. & Hoppel, C.L. Cardiolipin: characterization of distinct oxidized molecular species. *J. Lipid Res.* **52**, 125–135 (2011).
54. Adelson, P.D., Dixon, C.E., Robichaud, P. & Kochanek, P.M. Motor and cognitive functional deficits following diffuse traumatic brain injury in the immature rat. *J. Neurotrauma* **14**, 99–108 (1997).
55. Shellington, D.K. *et al.* Polynitroxylated pegylated hemoglobin: a novel neuroprotective hemoglobin for acute volume-limited fluid resuscitation after combined traumatic brain injury and hemorrhagic hypotension in mice. *Crit. Care Med.* **39**, 494–505 (2011).
56. Mouton, PR. *Unbiased Stereology: a Concise Guide* (The John Hopkins University Press, 2011).